https://doi.org/10.1016/j.jes.2021.02.024

Ambient volatile organic compounds at a receptor site in the Pearl River Delta region: variations, source apportionment and effects on ozone formation

Yao Meng [1,#], Junwei Song [2,#], Lewei Zeng [4], Yingyi Zhang [1], Yan Zhao [3], Xufei Liu [4], Hai Guo [4], Liuju Zhong [3], Yubo Ou [3], Yan Zhou [3], Tao Zhang [3], Dingli Yue [3,], Senchao Lai [1,*]*

[1] The Key Lab of Pollution Control and Ecosystem Restoration in Industry Clusters, Ministry of Education, and Guangdong Provincial Key Laboratory of Atmospheric Environment and Pollution Control, School of Environment and Energy, South China University of Technology, Guangzhou 510006, China

[2] Institute of Meteorology and Climate Research, Karlsruhe Institute of Technology, Hermann-von-Helmholtz-Platz 1, Eggenstein-Leopoldshafen, Germany

[3] Guangdong Environmental Monitoring Center, State Environmental Protection Key Laboratory of Regional Air Quality Monitoring, Guangzhou 510308, China

[4] Department of Civil and Environmental Engineering, The Hong Kong Polytechnic University, Hong Kong

[*] **To Whom Correspondence should be addressed**

E-mail: sclai@scut.edu.cn (S. Lai) and (D. Yue)

[#] These authors contributed equally to this work.

to be submitted to Environmental pollution

Highlights

- Ambient VOCs were measured by an online GC-MS/FID system.
- Solvent usage, LPG usage and vehicle exhaust are main VOC sources.
- The formation of O_3 is anthropogenic VOC-limited with dominant contributions from aromatics.
- Frequent high-O_3 episodes revealed the importance of regional transport in photochemical pollution.

Abstract

We present the continuously measurements of volatile organic compounds (VOCs) at a receptor site (Wan Qing Sha, WQS) in the Pearl River Delta (PRD) region from September to November of 2017. The average mixing ratios of total VOCs (TVOCs) was 36.4 ± 27.9 ppbv with the dominant contribution from alkanes (55.6%), followed by aromatics (33.3%). The diurnal variation of TVOCs showed a strong photochemical consumption during daytime, which is related to the formation of ozone (O_3). Five VOC sources were resolved by the positive matrix factorization (PMF) model, including solvent usage (28.6%), liquid petroleum gas (LPG) usage (24.4%), vehicle exhaust (21.0%), industrial emissions (13.2%) and gasoline evaporation (12.9%). The regional transport air masses from the upwind cities of south China can result in the elevated concentrations of TVOCs. Lower ratios of TVOCs/NO_x (1.59 ± 1.12) suggested that the O_3 formation regime at WQS site was VOC-limited, which also confirmed by a photochemical box model with the master chemical mechanism (PBM-MCM). Furthermore, the observation on high-O_3 episode days revealed that frequent O_3 outbreaks at WQS were mainly caused by the regional transport of anthropogenic VOCs especially for aromatics and the subsequent photochemical reactions. This study provides valuable information for policymakers to propose the effective control strategies on photochemical pollution in a regional perspective.

Keywords: VOCs; PRD region; Source apportionment; O_3; Regional transport

1. Introduction

Volatile organic compounds (VOCs) play important roles in atmospheric environmental chemistry because they can affect regional air quality and human health and climate (Guo et al., 2017; Seinfeld and Pandis, 2006). VOCs can react with nitrogen oxides (NO_x = NO + NO_2) in the presence of sunlight leading to the production of tropospheric ozone (O_3) and thus trigger photochemical pollution (Atkinson, 2000). VOCs such as aromatic compounds and biogenic species are significant precursors for the formation of secondary organic aerosols (SOA) (Hallquist et al., 2009).

The sources of VOCs include biogenic and anthropogenic emissions. Biogenic VOCs mainly emitted from terrestrial plants, marine phytoplankton and other natural sources, which are regarded as the largest contributor of VOCs globally (Guenther et al., 2012). In urban and rural areas, anthropogenic VOCs can be dominant (Guo et al., 2017). Compared to biogenic VOCs, the sources of anthropogenic VOCs are often complex including vehicular exhaust, fuel evaporation, industrial emissions and biomass burning (Guo et al., 2017; Liu et al., 2008a). The emissions of anthropogenic VOCs depend largely on the energy consumption and industries. In many Chinese urban areas, vehicular emission is widely reported as one of the major sources of anthropogenic VOCs (Cai et al., 2010; Guo et al., 2011; Li et al., 2016; Lyu et al., 2016), while industrial emissions are the largest contributor of anthropogenic VOCs in highly industrialized regions (An et al., 2014; Mo et al., 2017). Urban and industrial emissions can contribute to the VOCs in downwind rural regions through long-range or regional transport (He et al., 2019; Russo et al., 2010b; Song et al., 2020; Tang et al., 2009).

It is well known that the photochemical formation of O_3 is non-linearly related to the precursors of VOCs and NO_x. The formation of O_3 is usually found to be VOC-limited in highly-polluted urban areas. While in the downwind rural regions, the O_3-VOC-NO_x relationship is not always constant with the changes of meteorological conditions such as tropical cyclones, continental anticyclones and mesoscale circulations (e.g., see-land breezes) (Ding et al., 2004; Guo et al., 2009; Wang et al., 2017; Zeren et al., 2019). The concentrations and photochemical reactivity of the VOC species are key factors in terms of the impacts on O_3 formation. Ozone formation potential (OFP) is widely used as a parameter to evaluate the combination effects by multiplying VOC concentration and its corresponding maximum incremental reactivity (MIR) factor (Carter, 1994). In addition, the observation-based model (OBM) coupled with Master Chemical Mechanisms (MCM) is developed as a powerful tool to investigate the O_3-VOC-NO_x relationship in recent years (He et al., 2019; Ling and Guo, 2014; Wang et al., 2017; Zeren et al., 2019). It can simulate the O_3 photochemical production and destruction based on observed ambient concentrations of O_3 and its precursors. He et al., (2019) used a photochemical box model incorporating the master chemistry mechanism (PBM-MCM) to investigate the photochemical formation of O_3 at a downwind rural site (Heshan) in the Pearl River Delta (PRD) during autumn 2014, and found that O_3 formation was VOC-limited. Wang et al., (2017) applied the PBM-MCM investigated the O_3 photochemistry at a downwind coastal site over the South China Sea (SCS). They revealed that the O_3 formation changed from transition (VOC and NO_x-limited jointly) to VOC-limited regime under the influence of sea-land breezes

96 from non-O_3 episode days to O_3 episode days.

97 As one of the most developed city clusters in China, the PRD region is densely
98 populated and rapidly developed with the pollution of O_3 and particulate matter{Lai,
99 2016 #174}. Over the last decade, a series of field campaigns and modeling studies
100 were performed in this region to understand the characteristics of VOCs including
101 abundances, composition, temporal variations, source contributions and chemical
102 reactivity, as well as the role in photochemical pollutant production (Barletta et al., 2008;
103 Guo et al., 2011; Guo et al., 2009; Ling et al., 2011; Liu et al., 2008b; Louie et al., 2013;
104 Yuan et al., 2013; Zeng et al., 2019; Zhang et al., 2013; Zou et al., 2015). Although
105 significant advances have obtained to understand the photochemical pollution
106 formation processes and to implement the control strategies, the PRD region is still
107 suffered from the frequent outbreaks of high-O_3 episodes. Even in the downwind areas
108 of PRD with sparse anthropogenic emissions, high-O_3 episodes were often observed as
109 well (He et al., 2019; Wang et al., 2017; Zeren et al., 2019). Here, we presented the
110 results of online VOCs observation at a receptor site in the PRD region in autumn 2017.
111 We intend (1) to characterize the concentration levels and diurnal variations of VOCs;
112 (2) to understand the contribution of VOC sources; and (3) to assess the impacts of
113 VOCs on O_3 formation with a focus on photochemical pollution periods.

114

115 **2. Experimental**

116 **2.1. Sampling site**

117 A field measurement was carried out at the site of Wan Qing Sha (WQS, 22°43'N,

113°33'E) from 1 September to 30 November 2017 (**Fig. S1**). WQS is a coastal site located at the Pearl River Estuary (PRE) connecting the land areas of PRD and the SCS. This site is located in the downwind area of urban Guangzhou (~50 km southeast to the city center of Guangzhou) and surrounded by several fast-developing cities (Dongguan, Shenzhen and Zhongshan, ~25-40 km). During autumn and winter seasons, this site can be regarded as a receptor site and frequently influenced by the air masses carrying large amounts of atmospheric pollutants from the upwind areas (Guo et al., 2011; Ling and Guo, 2014). It is an ideal site to study the characteristics of regional pollution in the PRD region.

2.2. Sampling and chemical analysis

Ambient VOCs were sampled and analyzed continuously by an online gas chromatography-mass spectrometry/flame ionization detector system (GC-MS/FID, Tianhong Instrument (TH-300B), Wuhan) with 1-h time resolution. The sampling tube inlet was 1.5 m above the rooftop (~15 m), and the outlet was connected to a PFA-made manifold with a by-pass pump drawing air at a rate of 15 L/min. Ambient air was continuously drawn through a PFA tube with an inner diameter of 7.6 cm. The air was then pre-concentrated by passing through a cold trap maintaining −80 °C for the removal of water and carbon dioxide (CO_2), and then trapped at −150 °C with an empty capillary column. After pre-concentration, the VOCs were desorbed by heating up to 100 °C rapidly and introduced into the GC-MS/FID system for analysis. The Photochemical Assessment Monitoring Station (PAMS) gas was used for the daily

calibration of GC-MS/FID system at 22:00 to 0:00 local time. The coefficients (R^2) of calibration curves were higher than 0.99 for each VOC species presented in this study. The method detection limits (MDLs) for VOC species ranged from 0.003-0.047 ppbv.

The trace gases including O_3, nitric oxide (NO), nitrogen dioxide (NO_2), carbon monoxide (CO), and sulfur dioxide (SO_2) were simultaneously monitored at this sampling site. Briefly, O_3 was monitored with a commercial UV photometric analyzer (Thermo 49i) with the lower detection limit of 1.0 ppbv. NO and NO_x were detected by a chemiluminescence analyzer (Thermo 42i) with the detection limit of 0.5 ppbv. CO was measured by a nondispersive infrared analyzer (Thermo 48i). SO_2 was measured by a pulsed UV fluorescence (Thermo 43i) with the detection limit of 0.5 ppbv. The meteorological parameters (i.e., temperature, relative humidity, wind direction, wind speed, and pressure) were recorded by a portable weather station (Model WXT520, Vaisala, Finland).

2.3. Models

2.3.1 Air mass back-trajectories

To trace the potential source regions of atmospheric pollutants, air mass back-trajectories are computed by using the Hybrid Single Particle Lagrange Integrated Trajectory (HYSPLIT) model (Stein et al., 2015). In this study, three-day air mass back-trajectories for each day were ran using HYSPLIT model with the arrival height of 200 m at every 6 hours for WQS site. Furthermore, we performed the air mass cluster analysis to categorize the back-trajectories into three groups for source origin analysis.

2.3.2 Positive matrix factorization (PMF) model

In this study, US EPA PMF 5.0 model was used for the source apportionment of VOCs (Norris, 2014). The PMF model is a multivariate factor analysis tool that decomposes a matrix of sample data into two matrices of factor contributions and factor profiles, which can be interpreted to explore the source types and contributions at a receptor site (Paatero, 1997; Paatero and Tapper, 1994). The decomposition of sample data matrix can be simplified as follows:

$$x_{ij} = \sum_{k=1}^{p} g_{ik} f_{kj} + e_{ij} \quad (1)$$

where x_{ij} is the jth species concentration measured in the ith sample, g_{ik} is the species contribution of the kth source to the ith sample, f_{kj} is the jth species fraction from the kth source, e_{ij} is the residual for each species and p is the total number of independent sources. Based on the least squares method, the number of sources and VOC source profiles of each species in the individual source can be obtained from PMF model calculation. The detailed operation of PMF model is given in supplement (**Text S1**).

2.3.3 Photochemical box model (PBM)

A photochemical box model incorporating the Master Chemical Mechanism (PBM-MCM) was used to simulate the photochemical formation of O_3. This model has been successfully applied to investigate the O_3 formation and its relationships with precursors (VOCs and NO_x) in previous studies (He et al., 2019; Lam et al., 2013; Ling and Guo, 2014; Lyu et al., 2016; Wang et al., 2017; Zeng et al., 2019). The sensitivity

of O_3 formation to its precursors was assessed using the relative incremental reactivity (RIR), which can be calculated using the following equation (Carter and Atkinson 1989):

$$RIR^S(X) = \frac{\left[P^S_{O_3-NO}(X) - P^S_{O_3-NO}(X-\Delta X)\right]/P^S_{O_3-NO}(X)}{\Delta S(X)/S(X)} \quad (1)$$

where $P^S_{O3-NO}(X)$ and $P^S_{O3-NO}(X-\Delta X)$ represent the O_3 formation potential in a base run with original concentrations, and in a run with a hypothetical change (ΔX) (10% in this study) in source/species X. In both runs, net O_3 production with titration by NO is considered. S(X) means the measured concentration of X, and ΔX is the concentration change of X caused by the hypothetical change ΔS(X). According to equation (1), a higher positive RIR value of a given precursor indicates a higher probability that O_3 production will be more effectively reduced by cutting down emissions of this precursor. A more detailed description of PBM-MCM is shown in supplement (**Text S2**).

3. Results and discussion

3.1. Data overview

The time series of air pollutant concentrations including VOCs, O_3, NO_x, CO as well as meteorological parameters during the campaign are shown **Fig. 1**. During the whole measurement period, the ambient temperature ranged from 13.2 to 36.4 °C with an average of 25.7 ± 4.6 °C. The relative humidity (RH) ranged from 24.0 % to 87.0 % with an average of 63.0 ± 13.2 %. The wind speed varied between 0.3 m/s to 5.4 m/s (average: 1.8 ± 0.8 m/s) with the prevailing wind direction of northeasterlies. The average concentrations of NO_x and CO were 26.2 ± 19.3 ppbv and 497 ± 158 ppbv,

206 respectively. The average concentrations of O_3 ranged from 2.33 to 192 ppbv with an
207 average of 34.9 ± 32.2 ppbv. According to the National Ambient Air Quality Standard
208 II of China, high O_3 episodes are defined as the days with maximum hourly average
209 mixing ratio of O_3 exceeding ~100 ppbv. It can be seen clearly in **Fig. 1** that high-O_3
210 days occurred during the sampling period. Specifically, 26 high-O_3 days were observed
211 during 1-3, 11-12, 15-21, 27-28 September, 23-27, 31 October, 1-2, 5, 9-10, 16, 29
212 November (**Table S1**). During most of the high O_3 days, we also observed high
213 concentrations of VOCs, suggesting that the O_3 formation is probably VOC-limited at
214 WQS site. We will further discuss the effects of VOCs on O_3 formation in **Section 3.5**
215 to illustrate the causes of these photochemical pollution episodes.

216 The mixing ratios of total VOCs (TVOCs) ranged from 4.51 to 190 ppbv with an
217 average of 36.4 ± 27.9 ppbv (**Fig. 1**). Among the measured VOCs, the group of alkanes
218 accounts for the largest fraction of TVOCs (55.6%), followed by aromatics (33.3 %),
219 alkenes (6.6 %) and alkyne (4.6 %). The dominance of alkanes followed by aromatics
220 is consistent with previous results widely reported in Chinese cities (Cai et al., 2010;
221 Liu et al., 2008b; Louie et al., 2013). The top 10 VOC species were ethane, propane, *n*-
222 butane, *i*-butane, *i*-pentane, *n*-pentane, ethyne, toluene, ethylbenzene and *m,p*-xylene,
223 totally accounting for 78.3% of TVOCs. Generally, ethane and ethyne are typical
224 species emitted from incomplete combustion of fossil fuel and biomass/biofuel (Guo et
225 al., 2007b; Lai et al., 2011; Tang et al., 2009). Their average mixing ratios were 2.40 ±
226 1.40 and 1.69 ± 1.10 ppbv, respectively. Propane, *i*-butane and *n*-butane are the major
227 components of liquid petroleum gas (LPG), which are widely regarded as tracers of

LPG usage (Blake and Rowland, 1995; Ling and Guo, 2014). The average mixing ratios were 4.63 ± 3.51, 2.22 ± 1.94 and 3.86 ± 3.74 ppbv for propane, *i*-butane and *n*-butane, respectively. The average concentration of two pentane isomers, *i*-pentane and *n*-pentane were 2.31 ± 3.05 and 1.67 ± 2.10 ppbv respectively, which were mainly emitted from gasoline evaporation and/or gasoline-fueled vehicle exhaust (Liu et al., 2008a; Liu et al., 2008b). In addition, high levels of aromatic hydrocarbons were observed with average mixing ratios of 5.96 ± 4.90 ppbv for toluene, 2.11 ± 1.15 ppbv for ethylbenzene and 2.75 ± 2.00 ppbv for *m,p*-xylene, respectively. Toluene, ethylbenzene and *m,p*-xylene (TEX) are common species emitted from traffic-related and industrial solvent usage in southern China (Zhang et al., 2012; Zhang et al., 2013). Overall, high concentrations of alkanes and aromatics suggest the important contributions of traffic emissions and industrial solvent usage to VOCs.

We also made a comparison of major VOC species (**Table S1**) with the offline measurement results at the same site from October to December 2007 (Ling et al., 2011). The mixing ratios of LPG tracers (propane, *i*-butane and *n*-butane) were significantly higher in 2017 than those observed in 2007. In contrast, we found lower concentrations of fossil fuel combustion-related species including ethane, ethylene, ethyne, *i*-pentane and benzene in 2017 compared to those in 2007. This could be attributable to the implementations of switching from fossil fuel/biofuel to LPG as vehicle fuel in the PRD region in recent years (Zhang et al., 2018). Besides, the mixing ratios of TEX were lower in 2017 than those in 2007. It suggests the effective reduction of VOCs emitted from industrial emissions in the PRD region. It should be noted that the concentration

and composition of VOCs could be also influenced by other factors such as the sampling period, meteorological conditions, analytical method and atmospheric reactions besides source emissions.

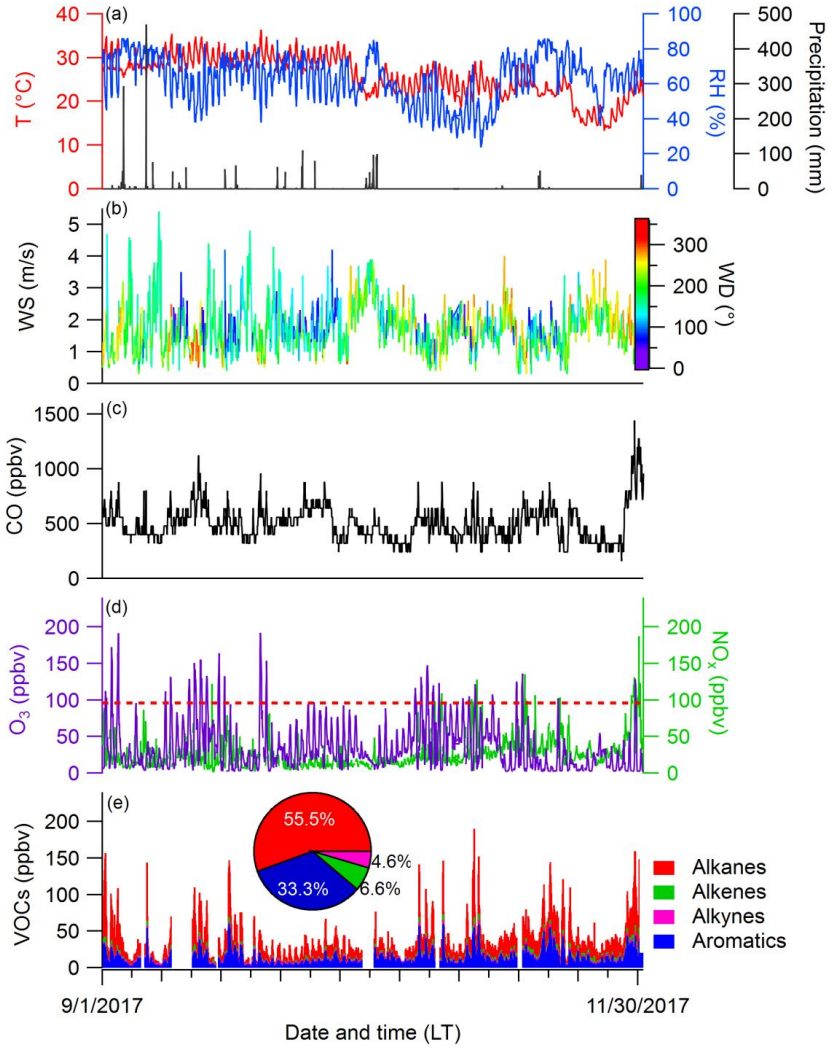

Fig. 1 Time series of air pollutants and meteorological conditions at WQS site from September to November 2017: (a) temperature (T), relative humidity (RH) and precipitation; (b) wind speed (WS) colored by wind direction (WD);(c) carbon monoxide (CO); (d) ozone (O_3) and nitrogen oxide (NO_x); the red dash line in (d) shows a threshold (O_3 > 100 ppbv) for the definition of high-O_3 days. (e) mixing ratios of VOCs

The pie chart shows the relative abundance of VOCs during the whole measurement period.

3. 2. Diurnal variations of VOCs, NO_x and O_3

Fig. 2 shows the diurnal variations of TVOCs, VOC groups, NO_x, and O_3 during the sampling period. The diurnal variations of VOCs at 22:00 to 0:00 local time (LT) were missing due to the daily calibration. In general, meteorological conditions play an important factor influencing the diurnal variations of atmospheric pollutants. In this study, lower wind speeds were observed during nighttime than daytime, indicating a more stagnant condition in favor of air pollutant accumulation during nighttime (**Fig. S2**). In addition to meteorology, emission sources and chemical reactions can also influence the diurnal variations of air pollutants. The diurnal variation of TVOC concentration was characterized with a peak at 8:00 to 9:00 LT in the morning. This peak of TVOCs can be attributed to the strong emissions of traffics in the morning rush hours. Subsequently, the concentration of TVOCs decreased quickly during the daytime (10:00 to 18:00 LT), which is related to the strong photochemical consumption of TVOCs. After 19:00 LT, the concentration of TVOCs increased and then stayed constantly during nighttime. It is likely caused by the increase of traffic emissions during evening rush hours and the shrink of atmospheric boundary layer during nighttime. The groups of alkanes, aromatics and alkenes showed fast photochemical consumptions during daytime (10:00 to 18:00 LT). The diurnal variations of some representative VOC species were shown in **Fig. S3**. C_2 species (ethane, ethylene, ethyne), propane, *i*/*n*-butanes, *n*-pentane and benzene exhibited the highest concentrations in the morning rush hours (8:00-9:00 LT), which are related to traffic emissions. However, there were no obvious morning peaks observed for toluene,

ethylbenzene and xylene, indicating that they mainly came from other sources such as solvent usage rather than traffic emissions. After the morning rush hours, the concentrations of ethene, propane, *i*/*n*-butanes, *n*-pentane, the so call BTEX (benzene, toluene, ethylbenzene and xylene) and styrene showed significant decreases during daytime, whereas they showed higher concentrations but with relatively flat trends during nighttime. Ethene and BTEX are highly reactive species with OH radicals, and thus their fast decreases were due to strong photochemical reactions during daytime. However, the constant trends of reactive VOC species during nighttime could be due to reduced oxidation capacity and increased stagnant condition of the atmosphere.

Similarly, the NO_x concentration also peaked at 8:00-9:00 LT, following a decreasing trend during daytime. This suggests the strong traffic emissions in the morning rush hours, followed by the fast-photochemical consumption of both TVOCs and NO_x. The diurnal variation of O_3 showed an opposite trend with TVOCs and NO_x during daytime with the highest concentration during the afternoon (13:00-16:00 LT). This indicates that the consumptions of VOCs and NO_x result in the photochemical formation of O_3 during daytime. During nighttime, the reduction of O_3 was caused by the titration of NO ($NO + O_3 \rightarrow NO_2 + O_2$). We further investigated the diurnal variation of TVOCs/NO_x ratios, which have been widely used to determine the O_3 formation regime (Li et al., 2019; Liu et al., 2016; Seinfeld, 1989; Zou et al., 2015). Generally, VOC-limited regimes occur when TVOCs/NO_x ratios are lower than 8, while NO_x-limited regimes occur when TVOCs/NO_x ratios are larger than 8 (Li et al., 2019; Liu et al., 2016; Zou et al., 2015). In this study, the average ratio of TVOCs/NO_x was 1.59 ±

1.12 during the whole measurement period. Furthermore, high concentrations of O_3 were often observed with TVOCs/NO_x ratios of 1~6 from midday to afternoon (**Fig. S4**). These results suggest that O_3 formation is VOC-limited at WQS site.

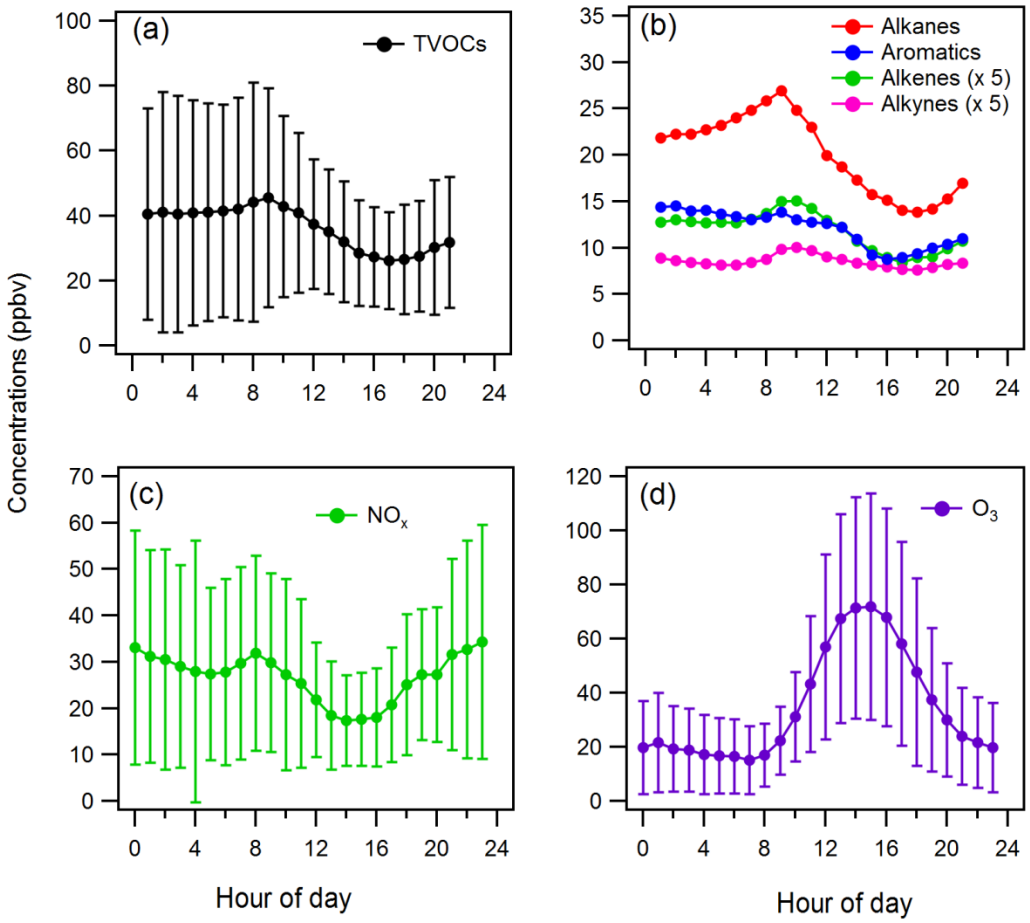

Fig. 2 Diurnal variations of TVOCs, VOCs groups, NO_x and O_3 at WQS site from September to November 2017: (a) TVOCs, (b) VOC groups, (c) NO_x and (d) O_3

The values of VOCs at 22:00-0:00 were excluded due to daily calibration.

3.3 Source identification of VOCs

The ratios of specific VOCs are useful indicators for investigating the sources of VOCs and the aging of air masses (Gilman et al., 2013; Guo et al., 2007a; Rossabi and Helmig, 2018). As *i*-pentane and *n*-pentane have similar sources and reactivity, their

ratio is widely used to reveal the VOC sources (Gilman et al., 2013; Rossabi and Helmig, 2018; Swarthout et al., 2013). In general, lower *i*-pentane/*n*-pentane ratios were observed in the areas highly-influenced by tropical forest fires (0.43-0.57) (Andreae and Merlet, 2001; Rossabi and Helmig, 2018), oil and natural gas operations (0.81-1.1) (Gilman et al., 2013; Swarthout et al., 2013). However, relatively high values of *i*-pentane/*n*-pentane ratios were reported for gasoline fuel evaporation (1.8-4.6), and in urban areas or tunnels with strong vehicle emissions (2.2-3.8) (Gentner et al.; Jobson et al., 2004; Russo et al., 2010a). In this study, *i*-pentane and *n*-pentane correlated well (R^2 = 0.88, **Fig. S5**), indicating that they originated from the common sources. The average ratio of *i*-pentane/*n*-pentane was 1.45 ± 0.45, which is close to the values for gasoline evaporation. Moreover, the average ratio of *i*-pentane/*n*-pentane was lower than that (4.16) observed at WQS site in 2007 (Ling et al., 2011). This implies the effective reduction of VOCs from gasoline-fueled vehicular emissions in the PRD region over the last decade.

Benzene is usually emitted from vehicle exhaust in the urban and rural areas (Li et al., 2017), while toluene mainly originated from the evaporation of industrial solvents used in paint, printing and coating (Yuan et al., 2010; Zhang et al., 2013). The ratio of toluene to benzene (T/B) is often used to identify the non-traffic source contributions to VOCs (Barletta et al., 2008; Elbir et al., 2007). When the ratio of T/B ratio is lower than 2, it indicates the strong influences from combustion sources including vehicle emissions and/or biomass burning. When the ratio of T/B is greater than > 2 indicate the major contributions from non-traffic sources especially paint solvent usage (Barletta

et al., 2008; Elbir et al., 2007). In this study, benzene showed a weak correlation with toluene (R^2 = 0.36, **Fig. S4)**, indicating that they came from different sources. Furthermore, the ratios of T/B ranged from 1.1 to 33.0 with an average of 7.3 ± 5.2, suggesting the important influence of solvent usage on VOCs at WQS.

The PMF model was used to resolve the source profiles and contributions of VOCs in this study. Five-factor was chosen as the optimal solution of PMF model results and the factor profile are shown in **Fig. 3**. Factor 1 is dominated by TEX, *n*-hexane, 3-methylpnene and *n*-heptane. TEX are the most common VOC species emitted from solvent usage in the PRD region (Zhang et al., 2012; Zhang et al., 2013). *n*-Hexane is used in the solvents for cooking oil extraction and as one of the cleaning reagents for shoe-making, furniture and textile. It can also be regarded as a tracer for household solvent usage (Guo et al., 2011). 3-methylpnene and *n*-heptane are also associated with the solvent usage in painting and varnishing (Guo et al., 2011; Ling and Guo, 2014). Therefore, factor 1 can be assigned to solvent usage. Factor 2 is characterized with high loadings of propane, *i*-butane and *n*-butane that are typical tracers of LPG usage (Blake and Rowland, 1995). As mentioned earlier, LPG has been widely used as the fuel for vehicles in the PRD regions in recent years (Zhang et al., 2018). This factor also has relative high percentages of ethene, propylene, *i*-pentane, which are likely associated with LPG usage. Therefore, we attributed to factor 2 to LPG usage. Factor 3 is identified with high abundances of ethane, ethylene, ethyne and benzene, which are typical tracers of incomplete combustion including fossil fuel and biomass burning (Guo et al., 2007b; Lai et al., 2011; Tang et al., 2009). In terms of the diurnal variations of ethane, propane,

ethylene, ethyne and benzene showing significant peaks in morning rush hours, it is reasonable to expect that they come from traffic emissions rather than biomass burning. Therefore, factor 3 is assigned to vehicle exhaust. Compared to factor 1, factor 4 is characterized with high loadings of ethylbenzene, *m/p*-xylene, *o*-xylene, and lower percentages of benzene and toluene. In addition to solvent usage, other industrial processes can also emit considerable amounts of aromatics in the PRD region (Zhang et al., 2012; Zhang et al., 2013). For example, xylenes are widely used in shoemaking, printing, packaging, toy and textiles industry in the PRD region (Guo et al., 2011; Ling et al., 2011). Therefore, we assigned factor 4 to industrial emissions. Factor 5 is dominated by high percentages of *i*-pentane and *n*-pentane, which were mainly emitted from gasoline evaporation (Guo et al., 2011; Ling et al., 2011). Therefore, factor 5 was regarded as gasoline evaporation.

Overall, solvent usage (28.6%) was the largest contributor to VOCs at WQS site, followed by LPG usage (24.4%) and vehicle exhaust (21.0%). We also compared the source contributions of VOCs with the previous study at WQS site in 2007 (Guo et al., 2011). Although lower contribution of solvent usage in 2017 than that in 2007 (46%) suggests the effective control in recent years, it is still an important source of VOCs at WQS site. The contribution of LPG was higher in 2017 than that (9%) in 2007, indicating the influence of LPG usage in the region over the last decade. In addition, the contribution of vehicle exhaust in 2017 was slightly lower than that (26%) in 2007.

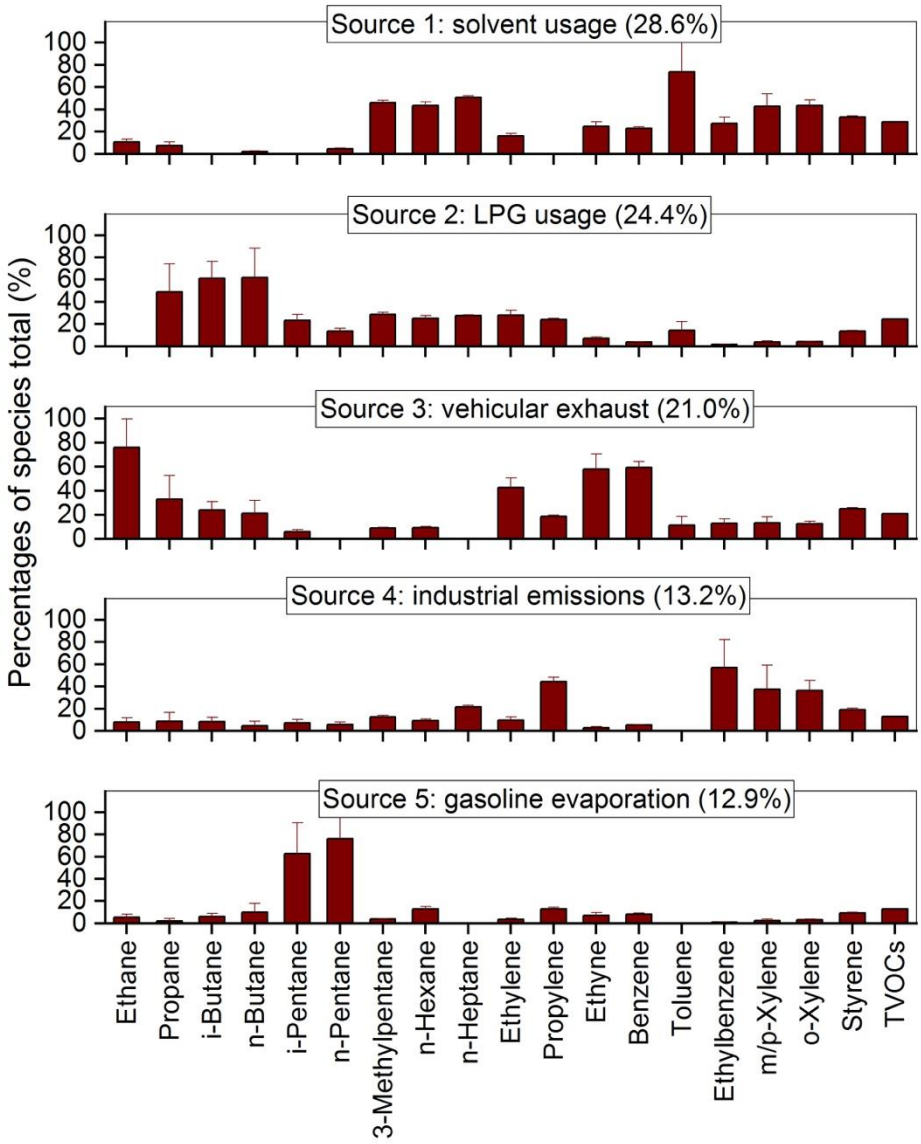

Fig. 3 Source profiles of VOCs identified by PMF model and the relative contributions of each source to the measured VOCs at WSQ site.

3.4 Atmospheric processing of VOCs

The ratios of VOCs with different photochemical lifetimes can be used to evaluate the atmospheric processes including photochemical aging and atmospheric transport (Guo et al., 2007b; Louie et al., 2013; Song et al., 2018). Ethyne and CO share common sources but have different photochemical lifetime with approximately 2 weeks for

391 ethyne and 2 months for CO. The ratio of ethyne/CO (E/C) have been widely used as a
392 measure of photochemical aging. In the PRD region, high ratios of E/C (5.6-7.5
393 pptv/ppbv) were reported for fresh combustion sources (Guo et al., 2007b; Louie et al.,
394 2013). In this study, the ratios of E/C ranged from 0.28 to 12.4 with an average of 3.49
395 ± 1.48, suggesting that the air masses at WQS site have experienced a certain extent of
396 photochemical aging.

397 The sources of ethylbenzene and *m/p*-xylene have similar sources such as solvent
398 usage, while they have different reactivities with OH radical. Therefore, the ratio of
399 *m/p*-xylene/ethylbenzene (X/E) can be used to assess the photochemical aging
400 processes. In this study, a good correlation (R^2 = 0.87, **Fig. S5**) was observed between
401 ethylbenzene and *m/p*-xylene, confirming that they came from the common sources.
402 Generally, the ratio of X/E is 3 for fresh emissions in urban environment (Monod et al.,
403 2001), while when the ratio lower than 3 indicates the occurrence of photochemical
404 aging. In this study, the ratios of X/E ranged from 0.68 to 2.23 with an average of 1.25
405 ± 0.30, suggesting the importance of photochemical aging and regional air mass
406 transport.

407 To investigate the atmospheric transport pathways, three-day air mass back-
408 trajectories were calculated using HYSPILIT model and further grouped into three
409 clusters (**Fig. 4**). The first cluster (Cluster-1) originated from the upwind areas of south
410 China (Jiangxi province) and upwind PRD cities (e.g., Dongguan and Huizhou),
411 accounting for 51.6% of total back-trajectories. In this cluster, the highest
412 concentrations of TVOCs (43.2 ± 30.1 ppbv) were observed, pointing to the influence

of upwind areas of south China. The second cluster (Cluster-2) accounted for 34.1% of total back-trajectories, which shows the air masses transported along the southeast coastal regions of China (Fujian and Zhejiang provinces). In the Cluster-2, the average mixing ratio of TVOCs was 32.9 ± 23.8 ppbv. In addition, the third cluster (Cluster-3) originated from the SCS, accounting for 14.3% of total air mass back-trajectories, in which lower level of TVOCs were observed (20.9 ± 17.6 ppbv). Although the compositions of measured VOCs showed no significant changes in different clusters, the predominance of alkanes and aromatics suggested the importance of traffic and industrial emissions by regional transport.

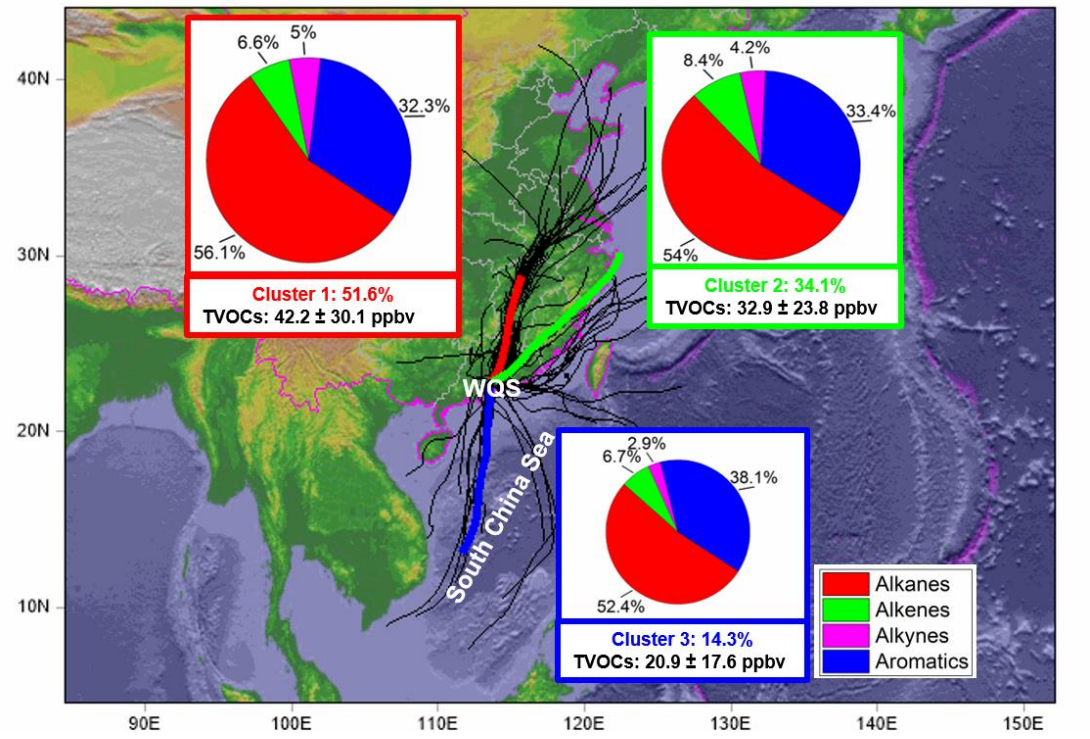

Fig. 4 Concentrations and composition of TVOCs in three air mass clusters (red: cluster 1; green: cluster 2, blue: cluster 3).

3.5. Effects of VOCs on O_3 formation

In order to estimate the potential effects of VOCs on O_3 formation, we calculated

firstly the OFP of VOC species as the following equation:

$$OFP_i = VOC_i \times MIR_i$$

where OFP_i and VOC_i are the OFP and the mixing ratios of VOC species i, and the MIR values are obtained from the study by Carter (1994). **Fig. 5** shows the contributions of different VOC groups and top 15 VOC species to the total OFP during the whole measurement period. Aromatics were the largest contributor, accounting for 57.1% of total OFP, followed by alkenes (22.3%) and alkanes (19.8%). As for individual VOC species, five abundant aromatics including toluene, ethylbenzene, *m*/*p*-xylene, styrene and o-xylene totally accounted for 55.6% of total OFP. Since toluene, ethylbenzene, *m*/*p*-xylene, styrene and o-xylene mainly contributed by the emissions of solvent usage, their high contributions to total OFP suggest that the reduction of regional industrial emissions could be the key to control photochemical O_3 pollution in the PRD region. In addition, ethene, propylene, propane and *i*/*n*-butanes also showed large contributions to total OFP, which are emitted from LPG usage. Even though LPG is commonly regarded as a 'cleaner' vehicle fuel, its usage can emit VOCs contributing to O_3 formation significantly. Therefore, LPG usage might also play important role in the formation of photochemical pollution.

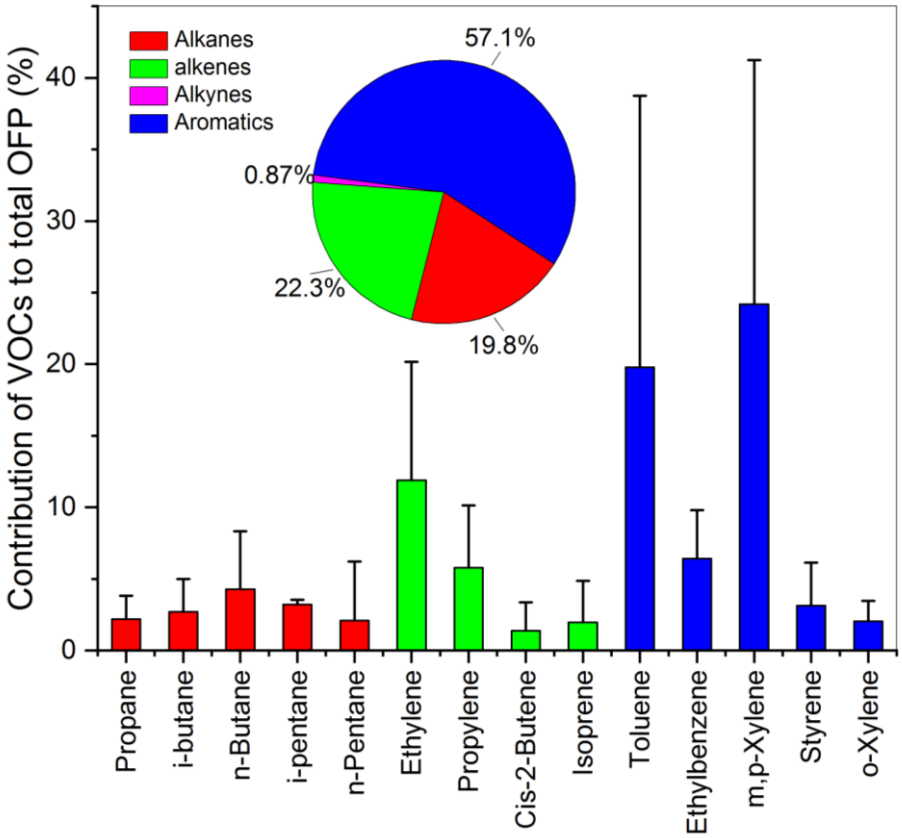

445

446 **Fig. 5** Contributions of major VOCs to total ozone formation potential (OFP) at WQS
447 site. The pie chart shows the relative contribution of each VOC group.

448

449 Furthermore, we simulated the O_3 formation processes by PBM-MCM and
450 calculated the RIR values of precursors to investigate their effects of on O_3 production.
451 **Fig. 6** shows the RIR of anthropogenic VOCs (AVOC), biogenic VOCs (BVOC), CO
452 and NO_x to investigate the sensitivity of O_3 to the changes of the precursors. As
453 mentioned in Section 3.1, we totally characterized 26 high-O_3 days during the entire
454 sampling period. Therefore, we classified the whole measurement period into O_3-
455 episode and non-O_3 episode days. Meanwhile, in order to better understand the
456 influence of regional transport in these photochemical pollution events, we further
457 classified these O_3-episode and non-O_3 episode days based on the influence of different

types of source origins as discussed above. On both O_3-episode and non-O_3-episode days, the RIR values of AVOC were always positive, indicating that the O_3 formation regime is AVOC-limited, which is in accordance with the discussion based on the TVOCs/NO_x ratios. In contrast, the RIR values of NO_x were always negative, suggesting that reducing NO_x levels would increase the O_3 production.

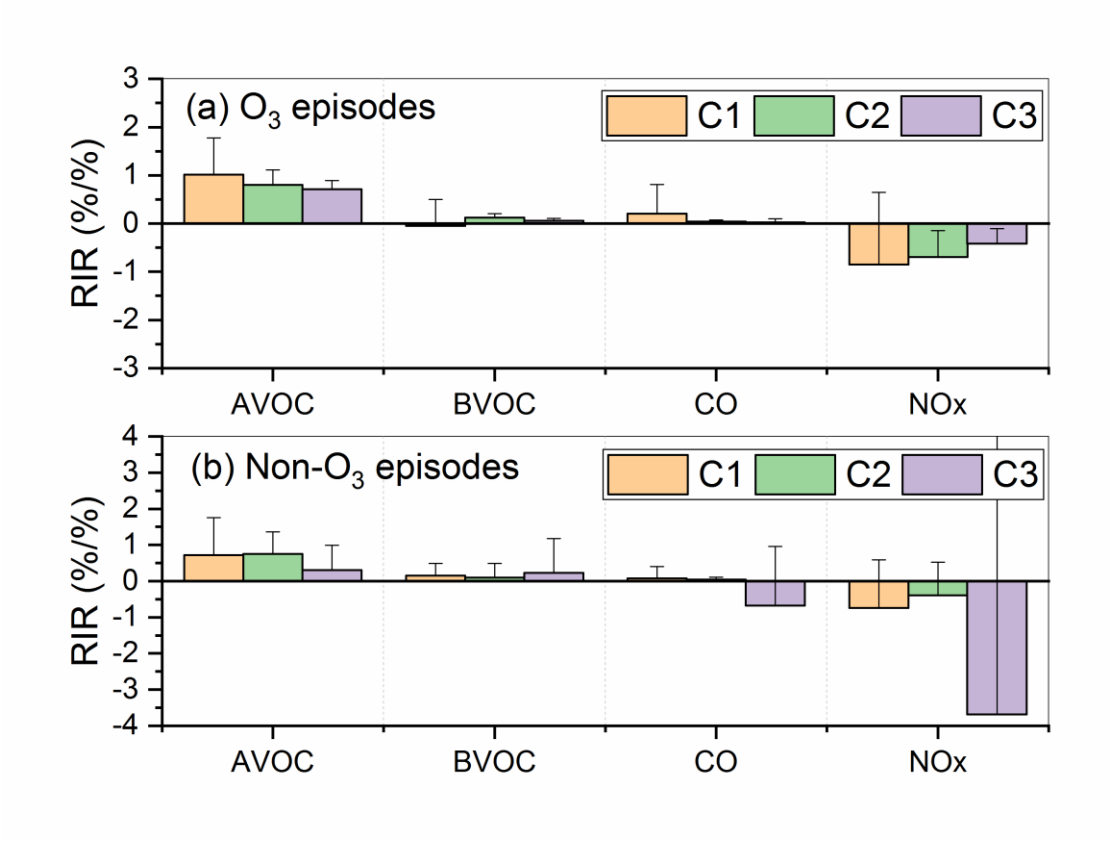

Fig. 6 Average RIR values of O_3 precursors during O_3 episodes and non-O_3 episodes. The precursors include anthropogenic VOCs (AVOC), biogenic VOCs (BVOC), CO, NO_x. C1, C2 and C3 represents the different influence of source origins.

Table 1 Summary of air pollutant concentrations and typical diagnostic ratios of VOCs during 26 high-O_3 days in three types of air mass clusters.

Clusters	Cluster-1 (n = 18)			Cluster-2 (n = 4)			Cluster-3 (n =4)		
Air mass origins	Southeast China/PRD			Southeast China coast			South China Sea		
	Mean	S.d[a]	Median	Mean	S.d	Median	Mean	S.d	Median
VOCs (ppbv)									
Alkanes	32.4	23.2	22.6	20.6	12.6	17.6	19.1	13.1	15.9
Alkenes	3.3	2.2	2.5	2.2	1.3	1.9	2.0	1.0	0.7
Alkyne	2.4	0.9	2.3	1.6	0.9	1.3	1.1	0.7	0.9
Aromatics	16.8	10.0	14.2	11.5	6.1	10.0	10.4	5.3	9.3
TVOCs	54.9	34.6	41.3	35.9	20.5	30.6	32.6	18.9	26.4
Air pollutants (ppbv)									
NO_x	35.4	22.1	29.0	27.2	16.0	24.7	21.4	10.5	18.8
O_3	56.0	41.0	46.7	49.1	42.2	37.3	53.8	52.1	32.0
CO	572	168	560	535	124	560	561	126	560
Diagnostic ratios									
Ethyne/CO	4.24	1.13	4.42	2.75	1.33	2.33	1.83	0.88	1.61
X/E	1.31	0.28	1.24	1.07	0.31	0.98	1.03	0.26	0.93

During all O_3-episode days, in addition to AVOC, CO also showed positive RIR values, indicating that reducing the levels of CO would lead to the decease of O_3 formation as well. Given the different origins of air mass clusters, the RIR value of AVOC and CO were higher in Cluster-1 than those in other two clusters (Cluster-2 and Cluster-3). This suggests that the formation of O_3 was mainly caused by regional transport of anthropogenic emissions from the upwind PRD urban regions. In particular, the occurrence frequency on high-O_3 days in Cluster-1 (n =18) was higher than that in Cluster-2 (n = 4) and Cluster-3 (n =4). Therefore, we suggested that the regional reduction of anthropogenic VOCs emissions would be effective for controlling the O_3 formation in the downwind PRD region. The variations of VOC and NO_x, CO and O_3 concentrations as well as the diagnostic ratios of E/C and X/E during O_3-episode days in different clusters were given in **Table 1**. In Cluster-1, higher concentrations of

TVOCs, NO_x, O_3 and CO were observed compared to those in another two clusters. Furthermore, the average ratios of E/C and X/E were higher in Cluster-1 than those in other two clusters (**Table 1**). The results indicate that more fresh emissions of anthropogenic pollutants transported regionally from the upwind PRD urban regions.

Besides, we also investigated the diurnal variations of O_3, TVOCs/NO_x and X/E ratios during O_3-episodes in different clusters (**Fig. 7**). In Cluster-1, the concentrations of O_3 were elevated with the increase of TVOCs/NO_x ratios from 10:00 to 16:00 LT during daytime. Correspondingly, the ratios of X/E showed fast decrease after 10:00 to 16:00 LT. The results suggest that the subsequent photochemical reactions lead to the formation of O_3 after the regional transport of anthropogenic emissions from upwind urban regions to WQS site. This result is in line with the recent findings that the downwind regions (PRE) can be act as a sink area of O_3 in the PRD region resulting from the transported air pollutants and intensive photochemical reactions (Zeren et al., 2019). Compared to Cluster-1, Cluster-2 had lower concentrations of O_3 during daytime (10:00-16:00) with the corresponding weak decrease of X/E ratios, indicating less photochemical reactions when WQS site was influenced by the air masses from Southeast coastal regions. However, in Cluster-3, we found that TVOCs/NO_x ratios showed fast decrease from 10: 00 to 12:00 with continuously increase of O_3. This is likely related to the shift of sea-land breezes during daytime. As shown **Fig. 7c**, a slightly increase of X/E ratios were observed in morning hours (7:00-9:00 LT), which is likely related to fresh emissions from the land air. In contrast, the ratios of X/E showed decrease continuously from 10:00 to 16:00, suggesting the photochemical

aging under the influence of SCS air. However, the limited number of high-O_3 days under the influence of air masses from the SCS cannot sufficiently demonstrate the effects of sea-land breezes on O_3 formation in this study. More long-term field measurements and modeling studies are necessary to investigate the role of sea-land breezes in photochemical pollution in the PRD region.

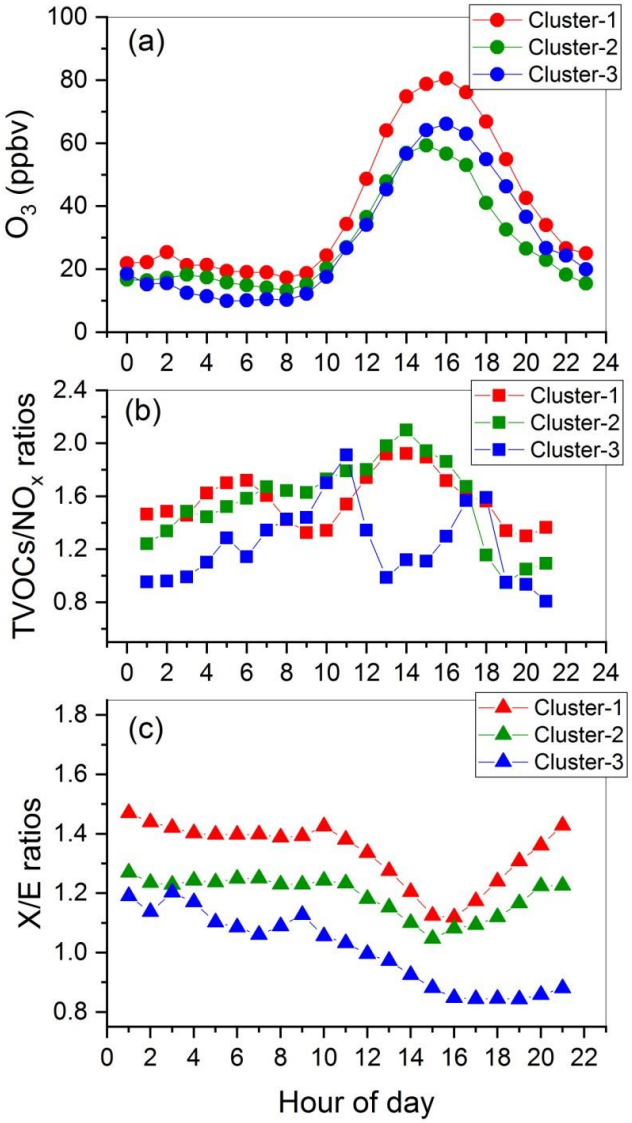

Fig. 7 Diurnal variations of O_3 concentrations, TVOCs/NO_x ratios and *m,p*-xylene/ethylbenzene (X/E) ratios during high-O_3 days with the influence of three air mass clusters.

4. Conclusions

In this study, VOCs were continuously measured at a receptor site in the PRD region from September to November 2017. The results showed that the dominant VOC species were alkanes and aromatics. The source apportionment results suggest solvent usage, LPG usage, vehicle exhaust were the major contributors of VOCs. The air mass back-trajectories showed that the upwind south China was the major source region of VOCs. The ratios of VOCs/NO_x and the result of PBM-MCMs indicated that the photochemical O_3 formation was anthropogenic VOC-limited at WQS site. Moreover, toluene, ethylbenzene, xylene, ethylene, propylene and *i/n*-butanes were the major contributors of total OFP. Finally, O_3 formation during the high-O_3 days were further investigated by PBM model simulation and diagnostic ratios of VOCs. The results suggest that frequent high-O_3 outbreaks were caused by the regionally transported pollutants followed by strong photochemical reactions. In future, more studies on O_3-VOC-NO_x relationship at downwind region are still needed, which is crucial for further improvement of regional photochemical pollution control strategies in the PRD region.

Acknowledgements

The authors thank the financial support of the National Key R&D Program of China (2017YFC0212802 and 2017YFC0212004).

References

An J, Zhu B, Wang H, Li Y, Lin X, Yang H, 2014. Characteristics and source apportionment of VOCs measured in an industrial area of Nanjing, Yangtze River Delta, China. Atmos. Environ. 97, 206-214.

Andreae MO, Merlet P, 2001. Emission of trace gases and aerosols from biomass burning. Global biogeochemical cycles 15 (4), 955-966.

Atkinson R, 2000. Atmospheric chemistry of VOCs and NO_x. Atmos. Environ. 34 (12), 2063-2101.

Barletta B, Meinardi S, Simpson IJ, Zou S, Sherwood Rowland F, Blake DR, 2008. Ambient mixing ratios of nonmethane hydrocarbons (NMHCs) in two major urban centers of the Pearl River Delta (PRD) region: Guangzhou and Dongguan. Atmos. Environ. 42 (18), 4393-4408.

Blake DR, Rowland FS, 1995. Urban Leakage of Liquefied Petroleum Gas and Its Impact on Mexico City Air Quality. Science 269 (5226), 953-956.

Cai C, Geng F, Tie X, Yu Q, An J, 2010. Characteristics and source apportionment of VOCs measured in Shanghai, China. Atmos. Environ. 44 (38), 5005-5014.

Carter WPL, 1994. Development of Ozone Reactivity Scales for Volatile Organic Compounds. J.air Waste Man.ass 44 (7), 881-899.

Ding A, Wang T, Zhao M, Wang T, Li ZK, 2004. Simulation of sea-land breezes and a discussion of their implications on the transport of air pollution during a multi-day ozone episode in the Pearl River Delta of China. Atmos. Environ. 38 (39), 6737-6750.

Elbir T, Cetin B, Cetin E, Bayram A, Odabasi M, 2007. Characterization of volatile organic compounds (VOCs) and their sources in the air of Izmir, Turkey. Environmental monitoring and assessment 133 (1-3), 149-160.

Gentner DR, Harley RA, Miller AM, Goldstein AH. Diurnal and Seasonal Variability of Gasoline-Related Volatile Organic Compound Emissions in Riverside, California. Environmental Science & Technology 43 (12), 4247-4252.

Gilman JB, Lerner BM, Kuster WC, De Gouw J, 2013. Source signature of volatile organic compounds from oil and natural gas operations in northeastern Colorado. Environmental science & technology 47 (3), 1297-1305.

Guenther AB, Jiang X, Heald CL, Sakulyanontvittaya T, Duhl T, Emmons LK, et al., 2012. The Model of Emissions of Gases and Aerosols from Nature version 2.1 (MEGAN2.1): an extended and updated framework for modeling biogenic emissions. Geosci. Model Dev. 5, 1471-1492.

Guo H, Cheng HR, Ling ZH, Louie PKK, Ayoko GA, 2011. Which emission sources are responsible for the volatile organic compounds in the atmosphere of Pearl River Delta? J. Hazard. Mater. 188 (1), 116-124.

Guo H, Jiang F, Cheng HR, Simpson IJ, Wang XM, Ding AJ, et al., 2009. Concurrent observations of air pollutants at two sites in the Pearl River Delta and the implication of regional transport. Atmos. Chem. Phys. 9 (19), 7343-7360.

Guo H, Ling ZH, Cheng HR, Simpson IJ, Lyu XP, Wang XM, et al., 2017. Tropospheric volatile organic compounds in China. Sci. Total. Environ. 574, 1021-1043.

Guo H, So KL, Simpson IJ, Barletta B, Meinardi S, Blake DR, 2007a. C_1-C_8 volatile organic

compounds in the atmosphere of Hong Kong: Overview of atmospheric processing and source apportionment. Atmos. Environ. 41 (7), 1456-1472.

Guo H, So KL, Simpson IJ, Barletta B, Meinardi S, Blake DR, 2007b. C_1–C_8 volatile organic compounds in the atmosphere of Hong Kong: Overview of atmospheric processing and source apportionment. Atmos. Environ. 41 (7), 1456-1472.

Hallquist M, Wenger JC, Baltensperger U, Rudich Y, Simpson D, Claeys M, et al., 2009. The formation, properties and impact of secondary organic aerosol: current and emerging issues. Atmos. Chem. Phys. 9 (14), 5155-5236.

He Z, Wang X, Ling Z, Zhao J, Guo H, Shao M, et al., 2019. Contributions of different anthropogenic volatile organic compound sources to ozone formation at a receptor site in the Pearl River Delta region and its policy implications. Atmos. Chem. Phys. 19 (13), 8801-8816.

Jobson BT, Berkowitz CM, Kuster WC, Goldan PD, Riemer D, 2004. Hydrocarbon source signatures in Houston, Texas: Influence of the petrochemical industry. Journal of Geophysical Research Atmospheres 109 (24), -.

Lai SC, Baker AK, Schuck TJ, Slemr F, Brenninkmeijer CAM, Velthoven PV, et al., 2011. Characterization and source regions of 51 high-CO events observed during Civil Aircraft for the Regular Investigation of the Atmosphere Based on an Instrument Container (CARIBIC) flights between south China and the Philippines, 2005-2008. J. Geophys. Res. -Atmos. 116 (D20), 1-15.

Lam SHM, Saunders SM, Guo H, Ling ZH, Jiang F, Wang XM, et al., 2013. Modelling VOC source impacts on high ozone episode days observed at a mountain summit in Hong Kong under the influence of mountain-valley breezes. Atmos. Environ. 81, 166-176.

Li B, Ho SSH, Gong S, Ni J, Li H, Han L, et al., 2019. Characterization of VOCs and their related atmospheric processes in a central Chinese city during severe ozone pollution periods. Atmos. Chem. Phys. 19 (1), 617-638.

Li B, Ho SSH, Xue Y, Huang Y, Wang L, Cheng Y, et al., 2017. Characterizations of volatile organic compounds (VOCs) from vehicular emissions at roadside environment: The first comprehensive study in Northwestern China. Atmospheric environment 161, 1-12.

Li J, Wu R, Li Y, Hao Y, Xie S, Zeng L, 2016. Effects of rigorous emission controls on reducing ambient volatile organic compounds in Beijing, China. Sci. Total. Environ. 557-558, 531-541.

Ling ZH, Guo H, 2014. Contribution of VOC sources to photochemical ozone formation and its control policy implication in Hong Kong. Environ. Sci. Policy 38, 180-191.

Ling ZH, Guo H, Cheng HR, Yu YF, 2011. Sources of ambient volatile organic compounds and their contributions to photochemical ozone formation at a site in the Pearl River Delta, southern China. Environ. Pollut. 159 (10), 2310-2319.

Liu B, Liang D, Yang J, Dai Q, Bi X, Feng Y, et al., 2016. Characterization and source apportionment of volatile organic compounds based on 1-year of observational data in Tianjin, China. Environ. Pollut. 218, 757-769.

Liu Y, Shao M, Fu L, Lu S, Zeng L, Tang D, 2008a. Source profiles of volatile organic compounds (VOCs) measured in China: Part I. Atmos. Environ. 42 (25), 6247-6260.

Liu Y, Shao M, Lu SH, Chang CC, Wang JL, Fu LL, 2008b. Source apportionment of ambient volatile organic compounds in the Pearl River Delta, China: Part II. Atmos. Environ.

42 (25), 6261-6274.
Louie PKK, Ho JWK, Tsang RCW, Blake DR, Lau AKH, Yu JZ, et al., 2013. VOCs and OVOCs distribution and control policy implications in Pearl River Delta region, China. Atmos. Environ. 76, 125-135.
Lyu XP, Chen N, Guo H, Zhang WH, Wang N, Wang Y, et al., 2016. Ambient volatile organic compounds and their effect on ozone production in Wuhan, central China. Sci. Total. Environ. 541, 200-209.
Mo Z, Shao M, Lu S, Niu H, Zhou M, Sun J, 2017. Characterization of non-methane hydrocarbons and their sources in an industrialized coastal city, Yangtze River Delta, China. Sci. Total. Environ. 593-594, 641-653.
Monod A, Sive BC, Avino P, Chen T, Blake DR, Sherwood Rowland F, 2001. Monoaromatic compounds in ambient air of various cities: a focus on correlations between the xylenes and ethylbenzene. Atmos. Environ. 35 (1), 135-149.
Norris G, R. Duvall, S. Brown, AND S. Bai. EPA Positive Matrix Factorization (PMF) 5.0 Fundamentals and User Guide. U.S. Environmental Protection Agency, Washington, DC, 2014.
Paatero P, 1997. Least squares formulation of robust non-negative factor analysis. Chemometr. Intell. Lab 37 (1), 23-35.
Paatero P, Tapper U, 1994. Positive matrix factorization: A non-negative factor model with optimal utilization of error estimates of data values. Environmetrics 5 (2), 111-126.
Rossabi S, Helmig D, 2018. Changes in Atmospheric Butanes and Pentanes and Their Isomeric Ratios in the Continental United States. J. Geophys. Res. -Atmos. 123 (7), 3772-3790.
Russo R, Zhou Y, White M, Mao H, Talbot R, Sive B, 2010a. Multi-year (2004–2008) record of nonmethane hydrocarbons and halocarbons in New England: seasonal variations and regional sources. Atmospheric Chemistry and Physics 10 (10), 4909-4929.
Russo RS, Zhou Y, White ML, Mao H, Talbot R, Sive BC, 2010b. Multi-year (2004–2008) record of nonmethane hydrocarbons and halocarbons in New England: seasonal variations and regional sources. Atmos. Chem. Phys. 10 (10), 4909-4929.
Seinfeld JH, 1989. Urban Air Pollution: State of the Science. Science 243 (4892), 745.
Seinfeld JH, Pandis SN. Atmospheric Chemistry and Physics: From Air Pollution to Climate Change. Wiley, J & Sons,Inc., Hoboken, New Jersey, 2006.
Song J, Zhang Y, Huang Y, Ho KF, Yuan Z, Ling Z, et al., 2018. Seasonal variations of C_1-C_4 alkyl nitrates at a coastal site in Hong Kong: Influence of photochemical formation and oceanic emissions. Chemosphere 194, 275-284.
Song J, Zhang Y, Zhang Y, Yuan Q, Zhao Y, Wang X, et al., 2020. A case study on the characterization of non-methane hydrocarbons over the South China Sea: Implication of land-sea air exchange. Sci. Total. Environ. 717, 134754.
Stein AF, Draxler RR, Rolph GD, Stunder BJB, Cohen MD, Ngan F, 2015. Noaa's Hysplit Atmospheric Transport and Dispersion Modeling System. B. Am. Meteorol. Soc. 96 (12), 2059-2077.
Swarthout RF, Russo RS, Zhou Y, Hart AH, Sive BC, 2013. Volatile organic compound distributions during the NACHTT campaign at the Boulder Atmospheric Observatory: Influence of urban and natural gas sources. Journal of Geophysical Research: Atmospheres 118 (18), 10,614-10,637.

Tang JH, Chan LY, Chang CC, Liu S, Li YS, 2009. Characteristics and sources of non-methane hydrocarbons in background atmospheres of eastern, southwestern, and southern China. J. Geophys. Res. -Atmos. 114.

Wang Y, Guo H, Zou S, Lyu X, Ling Z, Cheng H, et al., 2017. Surface O_3 photochemistry over the South China Sea: Application of a near-explicit chemical mechanism box model. Environ. Pollut. 234, 155-166.

Yuan B, Min S, Lu S, Wang B, 2010. Source profiles of volatile organic compounds associated with solvent use in Beijing, China. Atmospheric Environment 44 (15), 1919-1926.

Yuan Z, Zhong L, Lau AKH, Yu JZ, Louie PKK, 2013. Volatile organic compounds in the Pearl River Delta: Identification of source regions and recommendations for emission-oriented monitoring strategies. Atmos. Environ. 76, 162-172.

Zeng L, Fan G-J, Lyu X, Guo H, Wang J-L, Yao D, 2019. Atmospheric fate of peroxyacetyl nitrate in suburban Hong Kong and its impact on local ozone pollution. Environ. Pollut. 252, 1910-1919.

Zeren Y, Guo H, Lyu X, Jiang F, Wang Y, Liu X, et al., 2019. An Ozone "Pool" in South China: Investigations on Atmospheric Dynamics and Photochemical Processes Over the Pearl River Estuary. J. Geophys. Res. -Atmos. 124 (22), 12340-12355.

Zhang Y, Wang X, Blake DR, Li L, Zhang Z, Wang S, et al., 2012. Aromatic hydrocarbons as ozone precursors before and after outbreak of the 2008 financial crisis in the Pearl River Delta region, south China. J. Geophys. Res. -Atmos. 117 (D15).

Zhang Y, Yang W, Simpson I, Huang X, Yu J, Huang Z, et al., 2018. Decadal changes in emissions of volatile organic compounds (VOCs) from on-road vehicles with intensified automobile pollution control: Case study in a busy urban tunnel in south China. Environ. Pollut. 233, 806-819.

Zhang YL, Wang XM, Barletta B, Simpson IJ, Blake DR, Fu XX, et al., 2013. Source attributions of hazardous aromatic hydrocarbons in urban, suburban and rural areas in the Pearl River Delta (PRD) region. J. Hazard. Mater. 250, 403-411.

Zou Y, Deng XJ, Zhu D, Gong DC, Wang H, Li F, et al., 2015. Characteristics of 1 year of observational data of VOCs, NO_x and O_3 at a suburban site in Guangzhou, China. Atmos. Chem. Phys. 15 (12), 6625-6636.